PHOTOMASK

BACUS—The international technical group of SPIE dedicated to the advancement of photomask technology.

N • E • W • S

AUGUST 2021
VOLUME 37, ISSUE 8

High resolution and uniform image reconstruction in a large field-of-view for EUV actinic mask review

H. Kim, U. Locans, R. Nebling, A. Dejkameh, D. Kazazis, Y. Ekinci, and I. Mochi,
Paul Scherrer Institute (PSI), Switzerland

ABSTRACT

Actinic EUV mask metrology is essentially needed for EUV lithography in the semiconductor device manufacturing process. At PSI, we are developing RESCAN, a coherent diffractive imaging (CDI)-based platform that can meet current and future mask inspection resolution requirements. In CDI, the diffraction patterns obtained by illuminating the sample with coherent light are recorded by a pixel detector, and these are used to reconstruct the complex-amplitude image of an object through an iterative phase retrieval algorithm. While in a conventional optical system, aberrations can compromise the final image's resolution, the CDI approach is inherently aberration-free. Nevertheless, a careful preprocessing of the diffraction signal is necessary to avoid artifacts in the reconstructed image. In particular, since our system works in reflection mode with an angle of incidence of 6° and uses a flat detector, it is necessary to correct the recorded diffraction patterns that are conically distorted due to the non-telecentricity. This paper discusses the impact of the diffraction data preprocessing on the reconstructed image quality and demonstrates the defect sensitivity improvement by applying an optimized data preprocessing pipeline in the RESCAN microscope. As a result, we achieve defect sensitivity down to 20 nm on the photomask and uniform image quality in a large field-of-view.

1. Introduction

For high-yield manufacturing and better quality of semiconductor chips, actinic patterned mask inspection (APMI) is an essential process in the extreme ultraviolet lithography (EUVL) ecosystem that is needed from the production to the deliveries on chucks. The feature sizes that have to be inspected and reviewed are becoming smaller with advanced mask materials. For these reasons, continuous development of the inspection technology is necessary to enable further progress of EUVL for future technology nodes[1-4].

RESCAN (Reflective-mode Scanning microscope) is a synchrotron-based APMI technology platform operating at the XIL-II beamline of the Swiss light source at PSI[5, 6]. It is capable of actinic inspections for both phase and amplitude defects on EUV photomasks[7]. It allows for detecting defects down to a size of about 50x50 nm^2[8]. Also, through pellicle imaging was demonstrated in RESCAN last year[9]. We currently plan an upgrade of the tool towards < 20 nm defect resolution to meet the 5 nm EUVL technology node and below[10].

The working principle of RESCAN is based on coherent diffractive imaging (CDI), which is a lensless imaging method[11]. Accordingly, RESCAN uses a diffraction recording detector and reconstruction algorithm instead of lenses to obtain the aerial image of the EUV mask. We also implement and develop the algorithm by considering various ptychography approaches to optimize the reconstruction speed and accuracy[12]. Ptychography is a scanning CDI technique that allows for the reconstruction of large field objects. Even though the probe size confines each detection field at every scan position, with the proper compromise between probe overlap and probe size, a large field of view (FOV) can be obtained.

By the physical nature of the reflection mode and the difficulty of using beam splitters at EUV wavelength, an angle between the sample and detector planes is unavoidable, and the imaging is non-telecentric similar to the imaging conditions in the EUV scanners. The reconstructed image distortion caused by the tilt is often neglected. However, as the feature size decreases, it becomes more critical for the image quality and defect sensitivity.

Table. 1. Specifications of the current version of the RESCAN tool

Wavelength	13.5 nm (±0.1nm)	Sample size	20 × 20 mm^2
$\lambda/\Delta\lambda$	1500	Inspect field area	200 × 200 μm^2
Flux	10^{12} (photons/s)	Resolution (pitch)	< 76 nm
Detector pixels	2048 × 2048	Δx (Eqn.(1))	< 38 nm
Detector size	27.6 × 27.6 mm^2	Sensitivity for	5 nm node

TAKE A LOOK INSIDE:

INDUSTRY BRIEFS
—see page 7

CALENDAR
For a list of meetings
—see page 8

SPIE.

11518-27

EDITORIAL

Spawned Innovation

Bryan Kasprowicz, HOYA Corporation

It can be argued that semiconductor manufacturing is the most complex industry reaching across many disciplines and requiring precision manufacturing to support what has become a critical piece of the world's infrastructure. Having been involved in this industry for quite some time, I often look for comparable products or manufacturing equipment. As one would suspect, they are hard to find; however, I managed to find a couple – the Boeing 787 Dreamliner and the Sleipnir from Heerema Marine Contractors (https://hmc.heerema.com/fleet/sleipnir).

The Dreamliner is impressively comparable to systems in our industry due to sourcing of materials or parts from hundreds of companies from more than a dozen countries. The industrial engineering and integration of such a project took on epic proportions, with many significant delays, but finally resulted in possibly the best airplane to date.

The airplane is self-explanatory, while the Sleipnir may need some background. It's a giant vessel, named after an eight-legged horse from Norse mythology, used for offshore heavy lifting – installing and transporting such things as gas/oil wells and HVAC installations. It is impressive because of its sheer size – 200m x 100m, displacement – 300,000 tons, onboard power generation – 96MW, lifting capability – 22 tons and dynamic positioning – can stay within 30cm in the open sea. I think even ASML would admire this size and capability!

Speaking of ASML, in context, these both compare to the complex industrialization and integration (including delays) and capability and size (the Dutch must use the philosophy of "go big or go home!") of what it took to develop and commercialize the EUV Scanner. This "single" tool, with many innovative components has allowed the Semiconductor Industry to continue to evolve and drove innovation in all other areas of materials and manufacturing.

A few of these areas include resists, where low EUV photon energy has caused much grief in patterning due to the infamous stochastic effects; atomic layer deposition, where only a few precisely atoms are create the thin layers of materials needed to evolve the transistor and interconnections; and etch, where extreme material selectivity and precision removal are needed to result in perfect profiles.

One specific area was the development of the EUV blank used in manufacturing of EUV masks. Development of EUV blanks got their start through the EUV LLC, and then SEMATECH's MBDC (Mask Blank Development Center) helped to solve some of the equipment-based defect issues. From there, the primary blank manufacturers accepted the challenge towards further improving the substrate, materials development, and commercialization. Today the availability of the standard tantalum-based EUV mask blank is in wide use in support of all EUV wafer manufacturing. And most recently, lithographers are reaching to the DUV past to help extend the EUV future by leveraging phase shift masks, as Eelco van Setten suggests in his PMJ paper this year titled, "High-NA EUVL Exposure Tool for EUV roadmap extension: Program Progress and Mask Interaction."

So, whether it's an airplane, offshore vessel, or EUV scanner, much innovation has spawned in many other areas. To learn more about some of the recent work, please consider virtually attending the BACUS and EUV Lithography Conference, September 27 - October 1.

N • E • W • S

BACUS News is published monthly by SPIE for *BACUS*, the international technical group of SPIE dedicated to the advancement of photomask technology.

Managing Editor/Graphics Linda DeLano

SPIE Sales Representative, Exhibitions, and Sponsorships Melissa Valum

BACUS Technical Group Manager Tim Lamkins

■ **2021 BACUS Steering Committee** ■

President
Emily E. Gallagher, *imec.*

Vice-President
Kent Nakagawa, *Toppan Photomasks, Inc.*

Secretary
Jed Rankin, *GLOBALFOUNDERIES Inc.*

Newsletter Editor
Artur Balasinski, *Cypress Semiconductor Corp.*

2021 Photomask + Technology Conference Chairs
Stephen P. Renwick, *Nikon Research Corp. of America*
Bryan S. Kasprowicz, *HOYA*

Members at Large
Frank E. Abboud, *Intel Corp.*
Uwe F. W. Behringer, *UBC Microelectronics*
Peter D. Buck, *Mentor Graphics Corp.*
Brian Cha, *Samsung Electronics Co., Ltd.*
Aki Fujimura, *DS2, Inc.*
Jon Haines, *Micron Technology Inc.*
Naoya Hayashi, *Dai Nippon Printing Co., Ltd.*
Bryan S. Kasprowicz, *HOYA*
Romain J Lallement, *IBM Research*
Patrick M. Martin, *Applied Materials, Inc.*
Jan Hendrik Peters, *bmbg consult*
Douglas J. Resnick, *Canon Nanotechnologies, Inc.*
Thomas Scheruebl, *Carl Zeiss SMT GmbH*
Thomas Struck, *Infineon Technologies AG*
Bala Thumma, *Synopsys, Inc.*
Anthony Vacca, *Automated Visual Inspection*
Vidya Vaenkatesan, *ASML Netherlands BV*
Andy Wall, *HOYA*
Michael Watt, *Shin-Etsu MicroSi Inc.*
Larry Zurbrick, *Keysight Technologies, Inc.*

SPIE.

P.O. Box 10, Bellingham, WA 98227-0010 USA
Tel: +1 360 676 3290
Fax: +1 360 647 1445
SPIE.org
help@spie.org

©2021

All rights reserved.

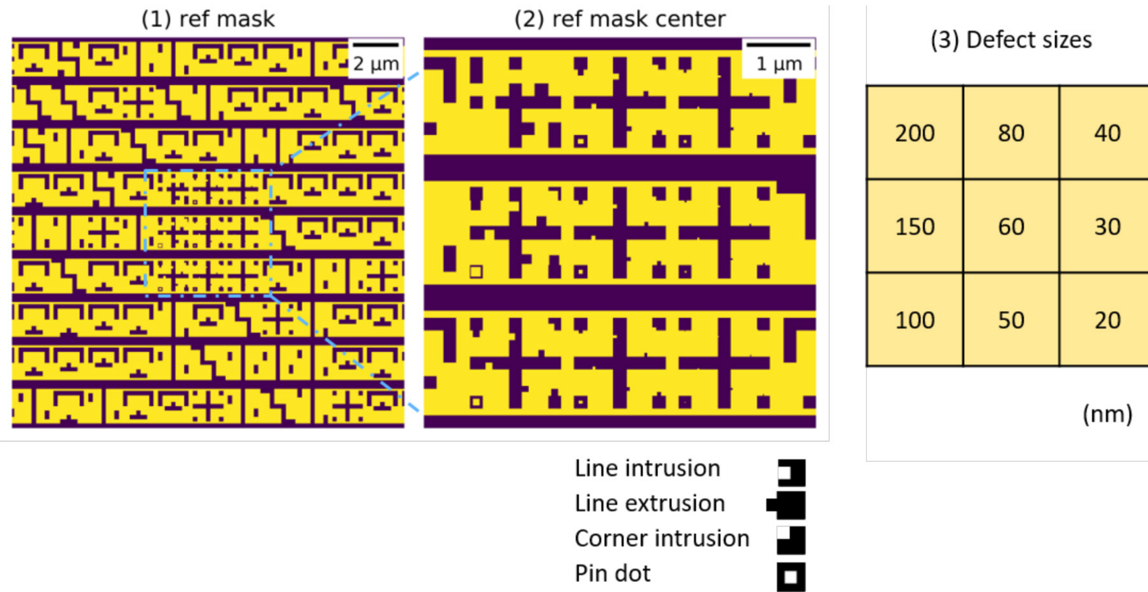

Figure 1. (1) The mask layout used in the present study (2) Zoom-in layout of the EUV mask at the central region and the types of programmed defects (3) Classification of the programmed defects by size in the nine regions in the center of the mask.

In this paper, we show and discuss the impact of the distortion of the diffraction patterns on the reconstructed aerial images and the benefits of using a diffraction correction algorithm resulting in improved image quality and thereby smaller defect sensitivity. It also removes the focus gradient observed in reconstructed images and increases the FOV.

2. Materials and Methods

RESCAN specifications

RESCAN is a synchrotron-based platform dedicated to actinic EUV mask review. Specifications of the current RESCAN tool are summarized in Table 1. The central wavelength is tunable ± 10% around 13.5 nm, which is limited by the optics. The beam generated by an undulator is spatially filtered by the pinhole and has temporal coherence of $\lambda/\Delta\lambda$=1500 after the monochromator. The EUV beam is focused by a multilayer-coated spherical mirror onto the EUV mask. The incident angle on the mask is 6° from the surface normal. The full collection NA is around 0.22 in the setup, but in this study, we use the CCD length of around 90%, which leads to NA = 0.19.

Resolution and sensitivity of RESCAN

In the setup, the scattered light from the sample to the detector has NA = sin(arctan($L/2D$)), where L = 27.6 mm is the detector size and D = 62 mm is the distance from the sample to the center of the detector. Therefore, the theoretical detectable defect size, Δx, can be defined as

$$\Delta x = k \cdot 0.6 \frac{\lambda}{NA} = \frac{k \cdot 0.6 \cdot \lambda}{\sin(\tan^{-1}(L/2D))}$$

which results in Δx = 37.5 nm for the present configuration of the RESCAN tool.

The resolution can be improved (to some extent) by using a larger detector with the same pixel size or by reducing the distance D with the smaller pixel size to increase the NA. In a given optical system, the process-related factor, k plays a substantial role in resolution to approach the theoretical limit. The most dominant aspect to obtain the minimum k includes the algorithm in the sense of how to utilize the collected diffraction data.

The different defect shapes yield different signals on the reconstructed image even though the defect size remains the same. Accordingly, we test RESCAN with various defect shapes placed on different locations on the mask pattern. In the Results section, we will show an example of the defect signal with different defect sizes for a particular defect type.

Sample structure and pattern description

The test mask sample is composed of HSQ (Hydrogen silsesquioxane) photoresist as an absorber with a thickness of 140 nm on top of a 40 pairs Mo/Si ML (multilayer). The programmed defects of various types are created with different sizes and located in the intricate logic pattern. The manufactured random logic pattern is shown in Fig. 1 (1). The critical dimension of the logic pattern is 200 nm. In the middle of the field, we added programmed defects in nine regions with different sizes ranging from 200 nm (top-left) to 20 nm (bottom-right) in Fig. 1 (2). The sizes of the defects in the nine regions are classified in Fig. 1 (3). We note that the absorber pattern is not a state-of-the-art material for EUV masks and results in lower contrast than conventional materials. It implies that the maximum capability of RESCAN can be little higher than the results shown in this paper.

Difference map (DM) reconstruction

In the present study, we use the difference map (DM), which is a phase retrieval algorithm frequently used in ptychography[13]. Compared to the other algorithms, the DM method is a relatively robust reconstruction method against image noise and probe positions errors[12]. In this paper, we keep the parameters the same in the DM algorithm for an exact comparison and see the impact of the newly added correction algorithm explained in the following Section.

Diffraction data correction (DDC) process

Spatially, the diffraction pattern lies on the cosine plane[14]. If the incident angle is normal to the surface and sample-to-detector distance D is relatively large, one can use the conventional processing of the diffraction patterns for the reconstruction. However, the non-telecentricity of the imaging setup, i.e., the tilted incident angle, leads to a diffraction image distortion and thus has an impact on the reconstructed image quality. The diffraction distortion effect is more clearly visible when the object is a grating, which yields the conical diffraction pattern[14, 15]. This image distortion can be modified by employing a rotation matrix inversely[16]. In addition, exact diffraction patterns lie on a spherical detector, and a flat detector leads to a gradient intensity fall. Nevertheless, the image by the flat detector can be simply modified. The intensity falls as a function

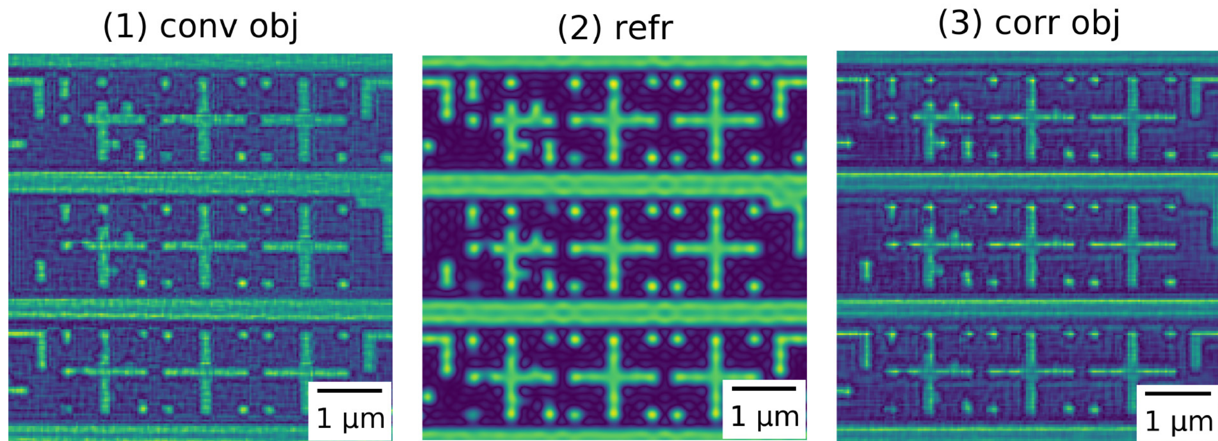

Figure 2. (1) the conventional object reconstructed without the DDC process. (2) Predicted aerial image of mask design (reference), and (3) the corrected object reconstructed with DDC process.

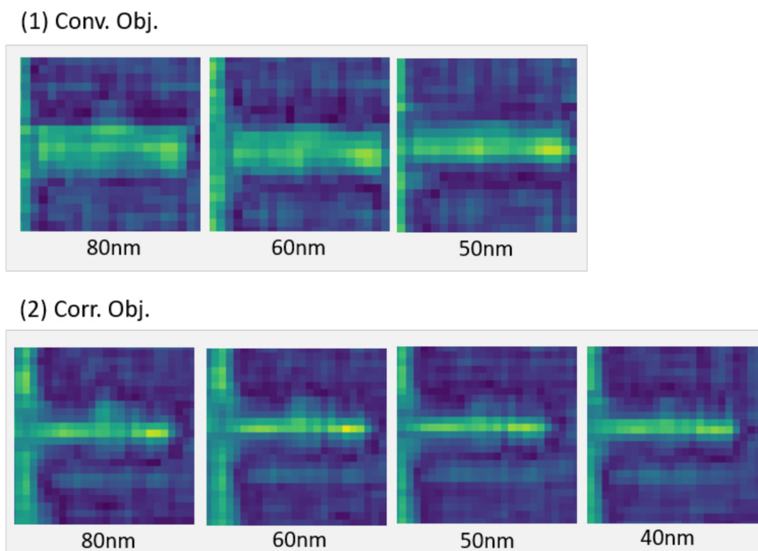

Figure 3. Zoom-in images of Fig. 2 (1) and Fig. (3) for line-extrusion defects on the horizontal lines for different defect sizes: (1) reconstructed defect images in a conventional object, and (2) reconstructed defect images in corrected object for different defect sizes.

of $1/r^2$, where r is the distance from the sample to the detector. In the DM algorithm, far-field diffractions are used by a fast Fourier transform (FFT) for phase retrieval iterations. The FFT assumes that the diffraction image plane and the plane in the frequency domain are parallel. Thus, preprocessing algorithm trims the modified diffraction data to comply with the FFT rules.

3. Results and Discussion

Reconstruction comparison and defect sensitivity

We reconstructed areal images of the EUV mask with and without the diffraction data correction (DDC) process using the same dataset of the diffraction patterns and same reconstruction parameters. The obtained images of the EUV mask with and without the DDC are compared in Fig. 2. The image shown in Fig. 2 (1) is the reconstruction without the DDC process. In Fig. 2 (3), the corrected object is the one with the DDC process. Fig. 2 (2) shows the Fourier-frequency filtered image of the mask layout in the given optical setup for die-to-database comparison. Comparing the above images in detail, the line-extrusion defects on the horizontal lines are zoomed-in in Fig. 3 for different defect sizes in both conventional and corrected objects. The defects in the corrected objects displayed in Fig. 3 (2) are more visible than the defects in the conventional object in Fig. 3 (1).

In Fig. 4, the intensity curves across the patterns to profile the line-extrusion defects in the corrected objects are shown. The line-extrusion defects on both horizontal and vertical lines (H-line and V-line, respectively) are measured near the line-edges. The intensity pops up where a defect is presented.

In Fig. 4, the two maximum intensity values in a curve are presented with red straight- and red dot lines, respectively. The red straight-lines denote the intensity maximum on the half-left side for H-line and on the half-top side for V-line. These are the profiles near the line-edges that have no defects. On the other hand, the red dot-lines denote the intensity maximum that corresponds to the defect cross-sections near the line-edges, as shown on the half-right side of the H-line and half-bottom side of the V-line. The gap between the straight-line and the dot-line reveals

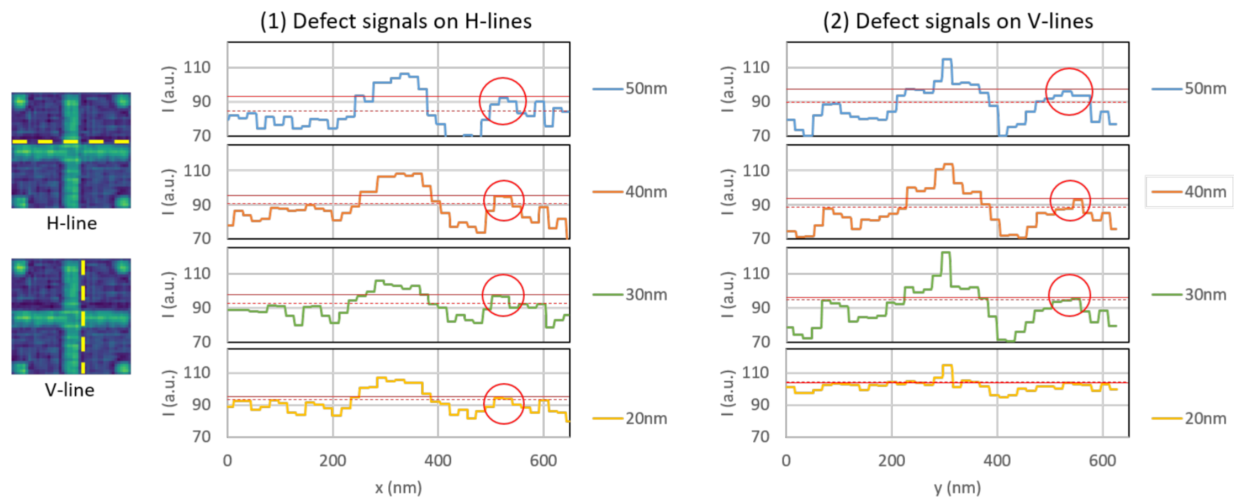

Figure 4. The cross-sectional profiles near the line-edges of the patterns: The defect signal curves are shown for the line-extrusion defects on both (1) horizontal (H-) and (2) vertical (V-) lines for different defect sizes from 50 nm to 20 nm. The two attached images on the left side denote the locations of the cross-sections for H- and V- lines.

the existence of the defect.

As a result, the defects on H-lines were detected down to 20 nm while the defect on V-line were detected down to 30 nm. The different defect sensitivities between H- and V-lines might come from the 3D effect of the 140-nm-high absorber pattern and the mask settlement on a chuck against the illumination direction that can lead to the defect hide behind the linewidth. We would like to further demonstrate for the defect sensitivity in different circumstances (i.e., a line-extrusion defect located far away from the center in a large FOV) to generalize the capability of the current version of RESCAN. In fact, the defect sensitivity can be improved by testing the TaBN absorber of 70 nm height and 70 pairs Mo/Si ML mask sample, providing less 3D effect and higher contrast than the test mask in this study.

Increased field of view

In ptychography, the field of view (FOV) is defined by the scan size, which, in principle, can be as large as the computational infrastructure allows. However, image quality control is more difficult as the reconstructed image size is increased because the optical defocusing effect is increased as a function of the object field size. Figure 5 (1) shows the reconstructed image in the large FOV. The degree of defocus is increased in a direction away from the center that the programmed defects are located.

Here, we found that the DDC process removes the defocus gradient effect in all reconstructed fields. Fig. 5 (2) shows the reconstructed image with the DCC process. The defocus removal effect is clearly visible, comparing the two images in the top right corners. The reconstructed image data having a large FOV can provide benefits for users to manage the reconstructed image on their purpose in the APMI tool. For example, because the reconstructed image is modularized, it is possible to pick up a reconstructed image at a specific location in the mask based on their rule-of-thumb even though the full mask reconstruction computation is not finished yet. Besides, the large FOV image can be convenient in various situations. Further research for the DDC process will demonstrate better image quality, higher defect sensitivity, and larger FOV.

4. Conclusions

The additional preprocessing that we implemented remaps the diffraction data on a sphere in the Fourier space and corrects the non-telecentricity of the imaging configuration. We demonstrated that by correcting the diffraction patterns recorded in RESCAN, we could significantly improve the defect sensitivity to enable the required EUV mask inspection technology for the 5-nm node. We demonstrated defect sensitivity down to 20 nm. In fact, the defect resolution and sensitivity achieved in this study can be further improved by using commercial EUV masks, which have higher contrast (approx. 10% higher) and less 3D effects (approx. 50% less) than the test mask used in this study. In addition, the resolution can be further improved 10% more than the result shown here if the algorithm is optimized to use full CCD, which might lead to defect sensitivity <18 nm. Furthermore, this implemented correction method removes the focal gradient, and thereby the reconstructed image FOV is enlarged, which allows for flexible post data processing. These improvements can also be applied for our plan to upgrade the RESCAN for high NA APMI toward below 5 nm EUVL node[10].

5. Acknowledgments

The authors would like to thank Markus Kropf, Michaela Vockenhuber, and Jose Gabadinho for their technical support at the XIL-II beamline. This project has received funding from the Electronic Component Systems for European Leadership Joint Undertaking under grant agreement No 783247-TAPES3. This Joint Undertaking receives support from the European Union's Horizon 2020 research and innovation program and the Netherlands, Belgium, France, Germany, Israel. Coauthors (A.T and R.N.) thank the Swiss National Science Foundation for financial support (SNF Grant Number: 200021_172768). Part of this research was performed at Swiss Light Source, Paul Scherrer Institut.

6. References

[1] S. Kim, R. Chalykh, H. Kim, S. Lee, C. Park, M. Hwang, J. Park, J. Park, H. Kim, J. Jeon, I. Kim, D. Lee, J. Na, J. Kim, S. Lee, H. Kim, and S. Nam, "Progress in EUV lithography toward manufacturing," **Proc. SPIE 10143,** 1014306 (2017).

[2] E. Verduijn, P. Mangat, O. Wood, J. Rankin, Y. Chen, F. Goodwin, R. Capelli, S. Perlitz, D. Hellweg, R. Bonam, S. Matham, N. Felix, and D. Corliss, "Printability and actinic AIMS review of programmed mask blank defects," **Proc. SPIE 10143,** 101430K (2017).

[3] T. Liang, Y. Tezuka, M. Jager, K. Chakravorty, S. Sayan, E. Frendberg, S. Satyanarayana, F. Ghadiali, G. Zhang, and F. Abboud, "EUV mask infrastructure and actinic pattern mask inspection," **Proc. SPIE 11323,** 1132310 (2020).

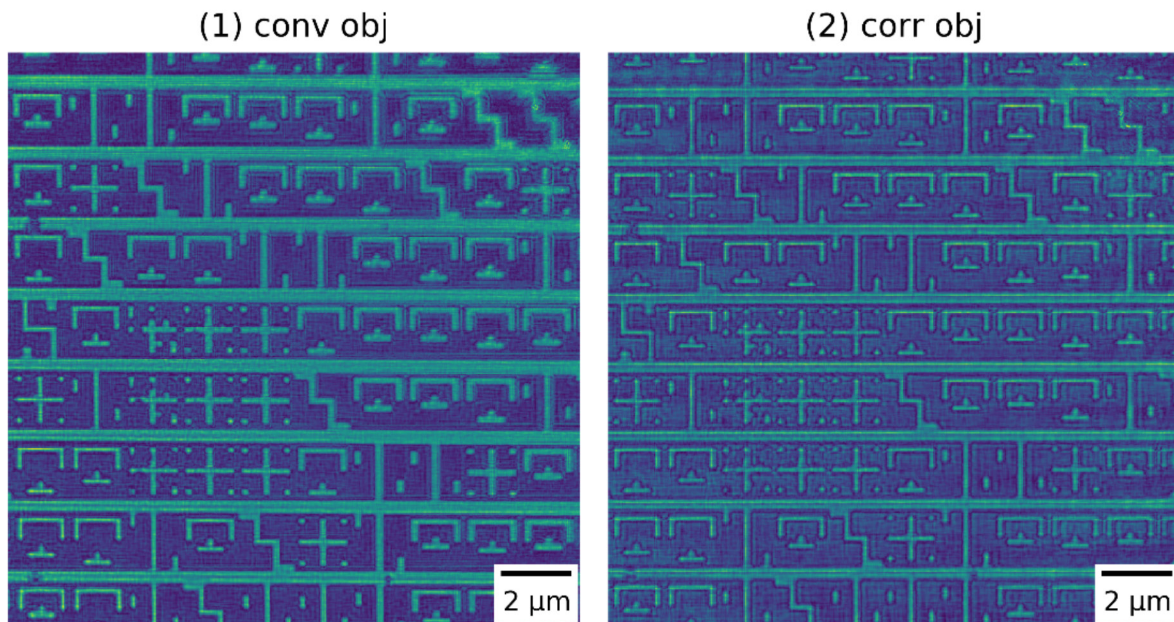

Figure 5. EUV mask images in a large FOV reconstructed (1) in a conventional way and (2) with the DDC processing, which results in an image with better defect sensitivity and without a focus gradient across the FOV.

[4] A. Tchikoulaeva, H. Miyai, T. Kohyama, K. Takehisa, and H. Kusunose, "Enabling EUVL high-volume manufacturing with actinic patterned mask inspection," **Proc. SPIE 11323,** 113231K (2020).

[5] P. Helfenstein, I. Mohacsi, R. Rajendran, and Y. Ekinci, "Scanning coherent diffractive imaging methods for actinic extreme ultraviolet mask metrology," *J. Micro/Nanolith. MEMS MOEMS* **15**(3) 034006 (2016).

[6] I. Mochi, P. Helfenstein, R. Rajeev, S. Fernandez, D. Kazazis, S. Yoshitake, and Y. Ekinci, "Actinic inspection of EUV reticles with arbitrary pattern design," **Proc. SPIE 10450,** 1045007-1045016 (2017).

[7] I. Mochi, S. Fernandez, R. Nebling, U. Locans, P. Helfenstein. R. Rajeev, A. Dejkameh, D. Kazazis, L. Tseng, and Y. Ekinci, "Absorber and phase defect inspection on EUV reticles using RESCAN," **Proc. SPIE. 10957,** 109570W (2019).

[8] I. Mochi, D. Kazazis, L. Tseng, S. Fernandez, R. Rajeev, U. Locans, A. Dejkameh, R. Nebling, and Y. Ekinci, "Lensless metrology for semiconductor lithography at EUV," **Proc. SPIE 11057,** 1105703 (2019).

[9] I. Mochi, M. Timmermans, E. Gallagher, M. Mariano, I. Pollentier, R. Rajendran, P. Helfenstein, S. Fernandez, D. Kazazis, and Y. Ekinci, "Experimental evaluation of the impact of carbon nanotube EUV pellicles on reticle imaging," *J. Micro/Nanolith. MEMS MOEMS* **18**(1) 014002 (2019).

[10] I. Mochi, H. Kim, U. Locans, A. Dejkameh, R. Nebling, D. Kazazis, and Y. Ekinci, "Illumination control in lensless imaging for EUV mask inspection and review," **Proc. SPIE 11323,** 113231I-1 (2020).

[11] J. Fienup, "Reconstruction of a complex-valued object from the modulus of its Fourier transform using a support constraint," *J. Opt. Soc. Am. A* **4**(1) (1987).

[12] R. Nebling, I. Mochi, D. Kazazis, U. Locans, A. Dejkameh, and Y. Ekinci, "EUV reticle inspection using phase retrieval algorithms: a performance comparison," **Proc. SPIE. 11147,** 111470R (2019).

[13] P. Thibault, M. Dierolf, O. Bunk, A. Menzel, and F. Pfeiffer, "Probe retrieval in ptychographic coherent diffractive imaging," *Ultramicroscopy* **109**(4), 338-343 (2009).

[14] J. Harvey and R. Pfisterer, "Understanding diffraction grating behavior: including conical diffraction and Rayleigh anomalies from transmission gratings," *Opt. Eng.* **58**(8), 087105 (2019).

[15] D. Gardner, B. Zhang, M. Seaberg, L. Martin, D. Adams, F. Salmassi, E. Gullikson, H. Kapteyn, and M. Murnane, "High numerical aperture reflection mode coherent diffraction microscopy using off-axis apertured illumination," *Opt. Express* **20**(17), 19050-19059 (2012).

[16] M. Seaberg, B. Zhang, D. Adams, D. Gardner, H. Kapteyn, and M. Murnane, "Tabletop coherent diffractive imaging of extended objects in transmission and reflection geometry," **Proc. SPIE 8851,** 88510Y (2013).

N • E • W • S

Sponsorship Opportunities

Sign up now for the best sponsorship opportunities

Photomask Technology + EUV Lithography 2021 Digital Forum

Contact: Melissa Valum
Tel: +1 360 685 5596; **melissav@spie.org**

Advanced Lithography + Patterning 2022

Contact: Teresa Roles-Meier
Tel: +1 360 685 5445; **teresar@spie.org**

Advertise in the BACUS News!

The BACUS Newsletter is the premier publication serving the photomask industry. For information on how to advertise, contact:

Melissa Valum
Tel: +1 360 685 5596
melissav@spie.org

BACUS Corporate Members

Acuphase Inc.
American Coating Technologies LLC
AMETEK Precitech, Inc.
Berliner Glas KGaA Herbert Kubatz GmbH & Co.
FUJIFILM Electronic Materials U.S.A., Inc.
Gudeng Precision Industrial Co., Ltd.
Halocarbon Products
HamaTech APE GmbH & Co. KG
Hitachi High Technologies America, Inc.
JEOL USA Inc.
Mentor Graphics Corp.
Molecular Imprints, Inc.
Panavision Federal Systems, LLC
Profilocolore Srl
Raytheon ELCAN Optical Technologies
XYALIS

Industry Briefs

STMicroelectronics Manufactures First 200mm Silicon Carbide Wafers

Shannon Davis, July 27, 2021

STMicroelectronics announced it has manufactured the first 200mm (8-inch) Silicon-Carbide (SiC) bulk wafers for prototyping next-generation power devices from its facility in Norrköping, Sweden. The transition to 200mm SiC wafers marks an important milestone in the capacity build-up for ST's customer programs in automotive and industrial sectors and will consolidate ST's lead in the disruptive semiconductor technology that allows for smaller, lighter, and more efficient power electronics with a lower total cost of ownership.

https://www.semiconductor-digest.com/stmicroelectronics-manufactures-first-200mm-silicon-carbide-wafers/

Intel Charts Manufacturing Course to 2025

Brian Santo, July 27, 2021

Intel CEO Pat Gelsinger announced a detailed roadmap for node progression. 10 nanometers will continue to be 10 nanometers — Intel is stuck with that. But the next version of 10 nm, aka SuperFin, will instead be Intel 7, and 7 nm will henceforth be Intel 4 (no "nanometers"). There will then be an Intel 3, after which Intel will then cease even thinking in nanometers; after 3, Intel will be alluding to angstroms, starting with nodes it will call 20A and 18A.

Intel said it will "fully embrace" EUV lithography with Intel 4. The company will continue refining finFET technology through Intel 3; after that, starting with 20A, it will shift to a gate all-around (GAA) structure. Everyone working on advanced process nodes is anticipating moving from finFET to GAA. Intel has its own approach to GAA, however, that it's calling the ribbonFET.

https://www.eetimes.com/intel-charts-manufacturing-course-to-2025/#

Chip Shortages Grow For Mature Nodes

Mark Lapedus, July 22, 2021

The current wave of chip shortages is expected to last for the foreseeable future, particularly for a growing list of critical devices produced in mature process nodes. Chips manufactured at mature nodes typically fall under the radar, but they are used in nearly every electronic device. Many of these chips are hot and in tight supply with long lead times, while others are easy to find. It depends on the chip type, specification, and vendor.

In addition, some leading-edge chips, such as select memories and processors, are also in the same boat. Those chips tend to grab most of the attention, but the ones based on mature nodes are also important. Among the mature-node semiconductors in tight supply are CMOS image sensors, display driver ICs, flash memory controllers, microcontrollers (MCUs), power MOSFETs, and power management ICs (PMICs).

https://semiengineering.com/chip-shortages-grow-for-mature-nodes/

Join the premier professional organization for mask makers and mask users!

About the BACUS Group

Founded in 1980 by a group of chrome blank users wanting a single voice to interact with suppliers, BACUS has grown to become the largest and most widely known forum for the exchange of technical information of interest to photomask and reticle makers. BACUS joined SPIE in January of 1991 to expand the exchange of information with mask makers around the world.

The group sponsors an informative monthly meeting and newsletter, BACUS News. The BACUS annual Photomask Technology Symposium covers photomask technology, photomask processes, lithography, materials and resists, phase shift masks, inspection and repair, metrology, and quality and manufacturing management.

Individual Membership Benefits include:

- Subscription to BACUS News (monthly)
- Eligibility to hold office on BACUS Steering Committee

spie.org/bacushome

Corporate Membership Benefits include:

- 3-10 Voting Members in the SPIE General Membership, depending on tier level
- Subscription to BACUS News (monthly)
- One online SPIE Journal Subscription
- Listed as a Corporate Member in the BACUS Monthly Newsletter

spie.org/bacushome

CALENDAR

2021

SPIE Photomask Technology + EUV Lithography Digital Forum
27 September-1 October 2021
https://spie.org/conferences-and-exhibitions/puv

2022

Photomask Japan
25-27 April 2022
PACIFICO Yokohama
Yokohama, Kanagawa, Japan
www.photomask-japan.org

SPIE is the international society for optics and photonics, an educational not-for-profit organization founded in 1955 to advance light-based science and technology. The Society serves more than 255,000 constituents from 183 countries, offering conferences and their published proceedings, continuing education, books, journals, and the SPIE Digital Library in support of interdisciplinary information exchange, professional networking, and patent precedent. In 2019, SPIE provided more than $5 million in community support including scholarships and awards, outreach and advocacy programs, travel grants, public policy, and educational resources. spie.org

SPIE.
International Headquarters
P.O. Box 10, Bellingham, WA 98227-0010 USA
Tel: +1 360 676 3290
Fax: +1 360 647 1445
help@spie.org • spie.org

Shipping Address
1000 20th St., Bellingham, WA 98225-6705 USA

Managed by SPIE Europe
2 Alexandra Gate, Ffordd Pengam, Cardiff, CF24 2SA, UK
Tel: +44 29 2089 4747
Fax: +44 29 2089 4750
spieeurope@spieeurope.org • spieeurope.org

You are invited to submit events of interest for this calendar. Please send to lindad@spie.org.